Detection of subthreshold pulses in neurons with channel noise

Yong Chen,[1,2,*] Lianchun Yu,[1] and Shao-Meng Qin[1]

[1]*Institute of Theoretical Physics, Lanzhou University, Lanzhou* 730000, *China*

[2]*Key Laboratory for Magnetism and Magnetic materials of the Ministry of Education, Lanzhou University, Lanzhou* 730000, *China*

(Dated: November 16, 2008)

Neurons are subject to various kinds of noise. In addition to synaptic noise, the stochastic opening and closing of ion channels represents an intrinsic source of noise that affects the signal processing properties of the neuron. In this paper, we studied the response of a stochastic Hodgkin-Huxley neuron to transient input subthreshold pulses. It was found that the average response time decreases but variance increases as the amplitude of channel noise increases. In the case of single pulse detection, we show that channel noise enables one neuron to detect the subthreshold signals and an optimal membrane area (or channel noise intensity) exists for a single neuron to achieve optimal performance. However, the detection ability of a single neuron is limited by large errors. Here, we test a simple neuronal network that can enhance the pulse detecting abilities of neurons and find dozens of neurons can perfectly detect subthreshold pulses. The phenomenon of intrinsic stochastic resonance is also found both at the level of single neurons and at the level of networks. At the network level, the detection ability of networks can be optimized for the number of neurons comprising the network.

PACS numbers: 87.19.lc, 87.19.ln, 87.16.Vy, 87.19.lb, 05.40.-a, 07.05.Tp

I. INTRODUCTION

It is well known that neurons are subject to various kinds of noise. Intracellular recordings of cortical neurons *in vivo* consistently display highly complex and irregular activity [1], resulting from an intense and sustained discharge of presynaptic neurons in the cortical network. Previous studies have suggested that this tremendous synaptic activity, or synaptic noise, may play a prominent role in neural information transmission as well as in neural information processing [2]. For example, with stochastic resonance (SR), synaptic noise facilitates information transfer or allows the transmission of the subthreshold inputs [3]. Indeed, SR induced by synaptic noise has been extensively studied in a single neuron and neural populations both experimentally and numerically [4, 5, 6].

While the synaptic noise accounts for the majority of noise in neural systems, another significant noise source is the stochastic activity of ion channels. Voltage-gated ion channels in neuronal membranes fluctuate randomly between different conformational states due to thermal agitation. Fluctuations between conducting and non-conducting states give rise to noisy membrane currents and subthreshold voltage fluctuations. Recently, much effort has been devoted to this field and channel noise is now understood to have important effects on neuronal information processing capabilities. Studies show that channel noise alters action potential dynamics, enhances signal detection, alters spike-timing reliability, and affects the tuning properties of the cell [7, 8, 9, 10] (for review see [11]).

Detection of small signals is particularly important for animal survival [13]. Both experimental and numerical studies have found, as depicted by SR, that synaptic noise can enhance the detection of subthreshold signals in nonlinear and threshold-detecting systems. For channel noise, there have been many papers concentrating on SR induced by channel noise [14, 15], and their results suggest that neurons may utilize channel noise to process subthreshold signals. However, it is still unclear whether reliable detection of subthreshold signals could obtained for single neuron if neurons do utilize SR to process signals. On the other hand, as a intrinsic noise source of neurons, channel noise is mostly studied within single neurons. Since recent studies suggest that channel noise enhances synchronization of two coupled neurons[16], it is natural to ask whether channel noise could take effects in the network level.

In this study we focus on subthreshold pulse detection in neurons with channel noise. First, using the stochastic Hodgkin-Huxley (SHH) neuron model, we study the effects of channel noise on the response properties of a single neuron to subthreshold pulse input. We find that a SHH neuron fires spikes a higher than average level in response to a subthreshold stimulus. The average response time decreases while the variance increases as the channel noise amplitude increases. This result is explained well by the phase plane analysis method [17]. Then, we evaluate the subthreshold signal detection ability of a SHH neuron under the pulse detection scenario proposed by Wenning et al. [18]. They reported that colored synaptic noise can enhance the detection of a subthreshold input. However, since the total error is always greater than 0.5, they argued that biological relevance of pulse detection for a single neuron is questionable. In the case of channel noise, we come to a similar conclusion.

*Corresponding author. Email: ychen.ch@gmail.com

Therefore, we propose a feasible solution for a neuronal population to overcome this predicament. We find that subthreshold signal detection can be greatly enhanced with the neuronal networks we propose. The phenomenon of intrinsic SR induced by channel noise is also observed. We argue this SR may be a strategy that neural systems would take to optimize their detection ability for subthreshold signals.

Our paper is organized as follows. In Sec. II the stochastic version of the Hodgkin-Huxley neuron model is presented. In Sec. III, we focus on how the single neuron responses to subthreshold transient input pulse. Phase plane analysis method is applied to explain results presented. In Sec. IV, we present the simple scenario for pulse detection and demonstrate that the detection ability of a single neuron is limited. Then we introduce the network that could reliably detect subthreshold pulses. Discussions and conclusions are presented in Sec. V.

II. MODELS

A. Deterministic Hodgkin-Huxley Model

The conductance-based Hodgkin-Huxley (HH) neuron model provides a direct relationship between the microscopic properties of an ion channel and the macroscopic behaviors of a nerve membrane [19]. The membrane dynamics of the HH equations are given by

$$C_m \frac{dV}{dt} = -\left(G_K(V - V_K^{rev}) + G_{Na}(V - V_{Na}^{rev}) + G_L(V - V_L)\right) + I, \tag{1}$$

where V is the membrane potential. V_K^{rev} and V_{Na}^{rev}, V_L are the reversal potentials of (K) potassium and (Na) sodium, the leakage currents, respectively. G_K, G_{Na}, and G_L are the corresponding specific ion conductances. C_m is the specific membrane capacitance, and I is the current injected into this membrane patch. The conductance for potassium and sodium ion channels are given by

$$G_K(V, t) = \overline{g}_K n^4, \qquad G_{Na}(V, t) = \overline{g}_{Na} m^3 h, \tag{2}$$

where $\overline{g}_K$ and $\overline{g}_{Na}$ are products of two factors: an individual channel conductance γ_K and γ_{Na} respectively, and the channel densities ρ_K and ρ_{Na} respectively. $\overline{g}_K$ and $\overline{g}_{Na}$ give the maximum conductance when all channels are open. The gating variables, n, m, and h, obey the following equations,

$$\frac{d}{dt}n = \alpha_n(V)(1 - n) - \beta_n(V)n,$$
$$\frac{d}{dt}m = \alpha_m(V)(1 - m) - \beta_m(V)m,$$
$$\frac{d}{dt}h = \alpha_h(V)(1 - h) - \beta_h(V)h, \tag{3}$$

where $\alpha_x(V)$ and $\beta_x(V)$ ($x = n, m, h$) are voltage-dependent opening and closing rates and are given in Table I with the other parameters used in the following simulations.

TABLE I: Parameters and rate functions used in our Simulations.

C_m	Specific membrane capacitance	$1\mu F/cm^2$
V_K^{rev}	Potassium reversal potential	$-77mV$
V_{Na}^{rev}	Sodium reversal potential	$50mV$
V_L	Leakage reversal potential	$-54.4mV$
γ_K	Potassium channel conductance	$20pS$
γ_{Na}	Sodium channel conductance	$20pS$
G_L	Leakage conductance	$0.3mS/cm^2$
ρ_K	Potassium channel density	$20/\mu m^2$
ρ_{Na}	Sodium channel density	$60/\mu m^2$
α_n		$\frac{0.01(V+55)}{1-e^{-(V+55)/10}} ms^{-1}$
β_n		$0.125e^{-(V+65)/80} ms^{-1}$
α_m		$\frac{0.1(V+40)}{1-e^{-(V+40)/10}} ms^{-1}$
β_m		$4e^{-(V+65)/18} ms^{-1}$
α_h		$0.07e^{-(V+65)/20} ms^{-1}$
β_h		$\frac{1}{1+e^{-(V+35)/10}} ms^{-1}$

B. Stochastic Hodgkin-Huxley Model

The deterministic HH model describes the average behaviors of a larger number of ion channels. However, ion channels are random devices, and for the limited number of channels, statistical fluctuations play a role in neuronal dynamics [20]. To treat the consequent fluctuations in ion conductance, two kinds of methods are often employed.

One is the so-called Langevin method which characterizes channel noise with Gaussian white noise [21]. In this description, the voltage variables still obey Eqs. (1) and (2) but the gating variables are random quantities obeying the following stochastic differential equations,

$$
\begin{aligned}
\frac{d}{dt}n &= \alpha_n(V)(1-n) - \beta_n(V)n + \xi_n(t), \\
\frac{d}{dt}m &= \alpha_m(V)(1-m) - \beta_m(V)m + \xi_m(t), \\
\frac{d}{dt}h &= \alpha_h(V)(1-h) - \beta_h(V)h + \xi_h(t),
\end{aligned}
\tag{4}
$$

where the variables $\xi_n(t)$, $\xi_m(t)$, and $\xi_h(t)$ denote Gaussian zero-mean white noise with

$$
\begin{aligned}
\langle \xi_n(t)\xi_n(t') \rangle &= \frac{2}{N_K} \frac{\alpha_n(V)(1-n) - \beta_n(V)n}{2} \delta(t-t'), \\
\langle \xi_m(t)\xi_m(t') \rangle &= \frac{2}{N_{Na}} \frac{\alpha_m(V)(1-m) - \beta_m(V)m}{2} \delta(t-t'), \\
\langle \xi_h(t)\xi_h(t') \rangle &= \frac{2}{N_{Na}} \frac{\alpha_h(V)(1-h) - \beta_h(V)h}{2} \delta(t-t'),
\end{aligned}
\tag{5}
$$

where N_K and N_{Na} are the total number of K^+ and Na^+ channels. Note that in this description, a precondition is that n, m, and h should be in the interval $[0, 1]$. It has been argued that the Langevin method cannot reproduce accurate results (see [22] for detail). However, it is still an effective method and widely used for its low computational cost. Additionally, the trajectory of the phase point prior to a spike entails major changes in the variables V and m but the variables n and h are practically unchanged during the same epoch [23]. So, this recipe enables us to investigate system behaviors in the $V - m$ phase plane.
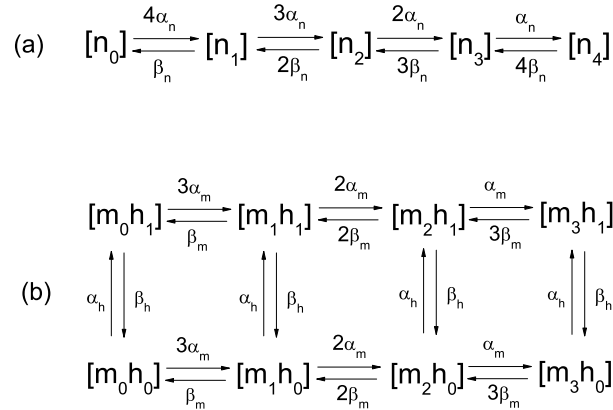

FIG. 1: Kinetic scheme for a stochastic potassium channel (a) and sodium channel (b). n_4 and m_3h_1 are open states, while the other states are non-conducting.

Another method is based on the assumption that the opening and closing of each gate of the channel is a Markov process. With this methods, the ion channel stochasticity is introduced by replacing the stochastic equations by the explicit voltage-dependent Markovian kinetic models for a single ion channel [8, 11, 12]. As shown in Fig. 1, the K^+ channels can exist in five different states and switch between these states according to the voltage dependence of the transition rates (identical to the original HH rate functions). n_4 labels the single open state of the K^+ channel. The Na^+ channel kinetic model has 8 states, with only one open state m_3h_1. Thus the voltage-dependent conductances for K^+ and Na^+ channels are given by

$$
G_K(V,t) = \gamma_K[n_4]/S, \qquad G_{Na}(V,t) = \gamma_{Na}[m_3h_1]/S,
\tag{6}
$$

where γ_K and γ_{Na} are defined as before, and $[n_4]$ refers to the number of open K^+ channels, $[m_3h_1]$ the number of open Na^+ channels, and S the membrane area of the neuron.

The numbers of open K^+ and Na^+ channels at a special time t is determined by the following formula: if the transition rate between state A and state B is r and the number of channels in these states is denoted by n_A and n_B, the probability that a channel switches within the time interval $(t, t + \Delta t)$ from state A to B is given by $p = r\Delta t$. Hence, for each time step, we determine Δn_{AB}, the number of channels that switch from A to B, by choosing a random number from the following binomial distribution,

$$P(\Delta n_{AB}) = \binom{n_A}{\Delta n_{AB}} p^{\Delta n_{AB}} (1 - p)^{(n_A - \Delta n_{AB})}. \tag{7}$$

Then we update n_A with $n_A - \Delta n_{AB}$, and n_B with $n_B + \Delta n_{AB}$. To ensure that the number of channels in each state is positive, starting at the beginning with the largest rate, we update these numbers sequentially, and so forth [22].

The noisiness of a cluster of channels can be quantified by the coefficient of variation (CV) of the membrane current. Under assumptions of stationarity (V is fixed), $CV = \{(1 - p)/np\}^{1/2}$, where n is the number of channels and p is the probability for each channel to be open. Thus the noisiness for a given population of voltage-gated channels is proportional to $n^{1/2}$ [11]. Accordingly, in this study, we introduce the membrane area S as a control parameter of the channel noise level. Given ion channel density, the level of channel noise decreases with an increase in membrane area.

The numerical integrations of stochastic equations for both the occupation number method and the Langevin method are performed by using forward Euler integration with a step size $0.01ms$. The parameters used in all simulations are listed in Table I. The occurrences of action potentials are determined by upward crossings of the membrane potential at a certain detection threshold $10mV$ if it has previously crossed the reset value of $-50mV$ from below.

III.   THE RESPONSE OF SHH NEURON TO A SUBTHRESHOLD TRANSIENT INPUT PULSE

The signal detection of transient subthreshold input pulses has received increasing attention in recent years [24, 25, 26] (see [18] for more references). In our study of the response of a SHH neuron, the transient input pulses are set with width $\delta t = 0.1ms$ and strength $I_0 = 5 \, \mu A/cm^2$.

Fig. 2(a) depicts the post-stimulus time histograms (PSTHs) of a SHH neuron with a membrane area S = 20, 200, and $1000\mu m^2$, respectively. Each stimulus was repeated 5000 times. The number of spikes observed in each bin (bin size = $0.1ms$) is normalized by the total number of stimuli and by the bin size. Thus, the PSTH gives the firing rate or the distribution of the firing probability as a function of time [27]. Obviously, there exists a peak over the spontaneous firing level in each curve and the peak lessens as the membrane area S increases. The higher the peak, the more sensitive neuron responses are to stimuli, which are activated by channel noise. The baselines show the average level of spontaneous firing due to channel noise. With a higher baseline, the number of spontaneous spikes increases. R. K. Adair has shown that the firing rate of a neuron with channel noise can be reduced by lowering the resting potential (Fig. 5 in Ref. [14]). In our case, the transient input pulse temporally hold the resting potential to a high state, thus gives a temporally higher firing rate over the spontaneous one. As the membrane area increases, since the fluctuations in membrane currents become smaller, the firings in response to the subthreshold signals as well as the noise-induced spontaneous firings are reduced, yielding reductions in heights of both the peaks and the baselines. It is noted that adjacent to the peak, there follows a time interval of about $10ms$ during which the firing rate is below its average level. We argue that this trough shape of the PSTH is due to refractoriness of the neurons [19]. If in a certain time interval the firing rate is higher than its average level, the firing rate in the following time range will be reduced because refractory effect prevents occurrence of the immediately following firings. The time interval of $10ms$ is in accordance with effective refractory period reported by other researchers [28].

To find the range in the membrane area which is more sensitive to a pulse than channel noise perturbation, we define signal-to-noise ratio (SNR) as the ratio of increased firing probability in response to input pulses to the probability for spontaneous firing in response to channel noise. [27]. As shown in Fig. 2(b), when the membrane area is smaller than $100 \, \mu m^2$, SNR remains very small. With increasing membrane area, SNR increases rapidly and reaches its maximum at about $400\mu m^2$. However, further increasing the membrane area leads to a decreasing in SNR. This figure clearly demonstrates the phenomenon of stochastic resonance. It is noted that as the membrane area increases, both the peak and the baseline of PSTH is reduced, so the occurrence of SR for SNR curve is a result of trade-off between neuron's sensitivity to subthreshold signals and rejection of spontaneous firings.

Next, we investigate how the channel noise affects the response time of neurons to subthreshold signals. It has been recently proposed that the first spikes which occur in, for example, cortical neurons, may contain information about a stimulus [29]. Thus, determinacy in response time of a neuron to signals is relevant to the information content, and how it is affected by channel noise would be an important question to explore [23]. The PSTH analysis provides us a first glimpse into it. The central positions of the PSTH peaks represent the mean response time, and the widths of the peaks represents the variances in response time. We see that as membrane area is increased, the central position of PSTH peak moves rightward, and its width is reduced simultaneously[see Fig. 2(a)]. This implies that as the membrane area increases, the mean response time increases but the variance in response time
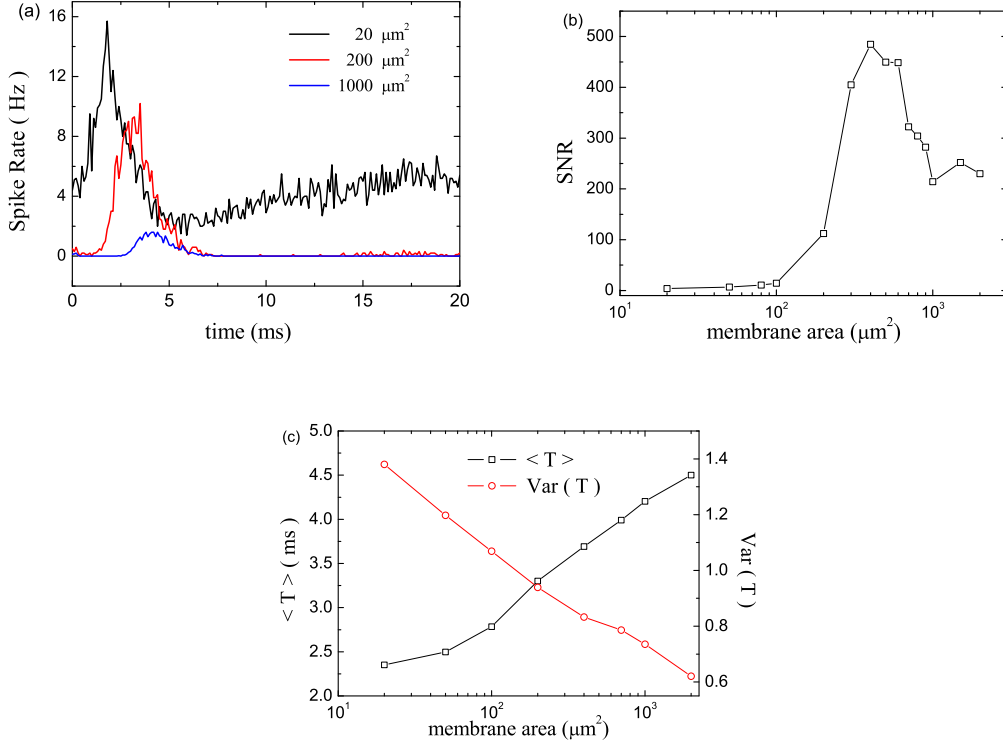
FIG. 2: (Color online) The response properties of a SHH neuron to subthreshold transient input pulses. (a) The PSTH of a SHH neuron with different membrane areas vs time. (b) SNR vs membrane area. (c) the mean response time and the variance of response time vs membrane area.

decreases. This is in consistent with the results obtained in the case of subthreshold inputs for external noise [30]. From 5000 times repeated trials, we directly calculate the mean and variance of response time for different membrane area, and plot them in Fig. 2(c). It seems that the increasing of $\langle T \rangle$ as well as the decreasing of $Var(T)$ is nearly in an exponential form.

To investigate the dynamic mechanism of a SHH neuron responding to transient input pulses, we performed a phase plane analysis with the Langevin simulation model described above. δt and I_0 for the input pulses are set as $1ms$ and $6\mu A/cm^2$, respectively. Fig. 3(a) shows the stable fixed point (SFP), part of the action potential trajectory (APT), and the unstable circles (UC) corresponding to different intensities of the input pulses in a noise-free HH model. The whole APT for $I_0 = 7.0$ is demonstrated in the inset of Fig. 3. Note that there exists a threshold in this system. The larger the intensity of input pulses, the further the system will be displaced from the SFP. If the displacement is larger than the threshold, an action potential is generated and the system comes back to the SFP along the APT. Otherwise, the system evolves along a relatively smaller unstable circle to the SFP [the color plots in Fig. 3(a)], and merely causes the subthreshold membrane potential fluctuations. When channel noise is involved, the system doesn't stay on the original SFP but fluctuates around the vicinity of SFP, which we call the resting area (RA) [the black area in Fig. 3(b)]. Occasionally, the system runs across the threshold due to perturbations in channel noise, then the system will evolve along a stochastic AP trajectory and a spontaneous action potential occurs. In the case of smaller membrane areas or larger RA, it is easier for the system to reach the AP trajectory under noise perturbation and produces more spontaneous firings (not shown).

To understand how the system responds to the pulse input with a amount of noise, we traced ten trajectories for pulses with firing and no firing, respectively. As shown in Fig. 3(c), in both cases, the system is displaced to an area around the threshold. Then after the stimulus is removed, the system jumps onto the APT to generate a spike or onto the unstable circle and returns back to the RA. This demonstrates the jumping is random. The more right the state is before jumping in phase plane, the greater possibility for it to jump onto the APT. The more left the state is before jumping, the more possible for the system to jump onto unstable circles. Since our discussions are limited to cases of a small amount of noise, noise cannot affect the length of the pulse displacement, and so the jumping area is determined by the initial state of the systems before the input pulse is applied (in our case, the state is described by two variables: V and m; n and h are not considered). The initial states with larger V and m are more likely to lead to an action potential [see the averaged initial positions for firing and no firing plotted in Fig. 3(c)]. Therefore we conclude that the response of the single SHH neuron to input pulses is state-dependent.
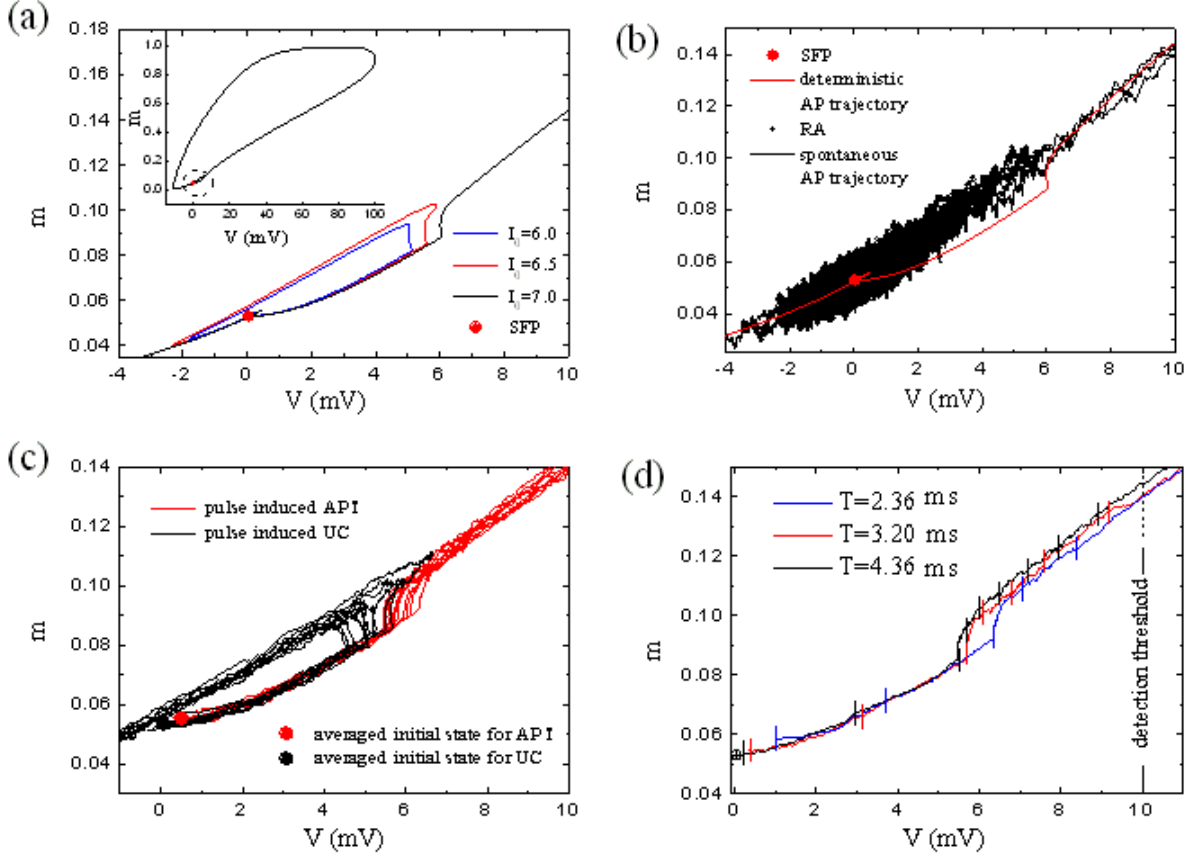
FIG. 3: (Color online) The phase plane analysis for the response properties of SHH neuron with Langevin simulations. (a) The action potential trajectory (APT) and the unstable circle of a noise-free HH neuron in the phase plane. Inset: the overall APT for $I_0 = 7.0$ and the position expanded in (a) (marked with dashed circle). (b) The stable area and the spontaneous APT for membrane area $S = 100\mu m^2$. (c) The noise-induced APT and the unstable circle (UC) for $S = 1000\mu m^2$. (d) Equitime labeling analysis of the response time to different initial states.

We also investigated the temporal response of the SHH neuron in the $V - m$ phase plane. In Fig. 3(d), the APTs with three different response times are traced and labeled with bars separated equally by $0.5ms$. The leftmost bars denote the time that the input pulse is applied, and the dashed line denotes the time that the spikes are detected. It shows that the system reaches a position closer to the detection threshold if the initial state is higher, and it will come into the outer side of the APT on which the system moves more quickly than the systems on the inside of the APT. As a result, this system presents a shorter response time to the input pulse, and vice versa. We see that the response time for a particular input pulse is dependent on the initial state of the system. In addition, one could deduce that it is the variance of initial state that results in the variance of the response time.

Next, we investigated how the change of membrane area (ie., the channel noise level) effects the distribution of initial state of the system, so that the response time exhibits statistics as shown in (c) of Fig. 2. The distributions of initial state for different membrane areas are described by the average and variance of V_{ini} and m_{ini}, which are calculated from 2000 firings in response to the pulses with Langevin simulation. It is seen from Fig. 4 that as the membrane area increases, both the average and variance of V_{ini} and m_{ini} decreases. In other words, with the decreasing of channel noise, the distribution of initial states in the phase plane moves left-down to the lower value and becomes narrower. As we discussed above, lower initial state leads to longer response time, and narrower distribution of initial states leads to smaller variance of the response time. Therefore, the average response time is prolonged and its variance is reduced if the membrane area is increased.

It is noted that because of large computational cost of our model, it is difficult to obtain the statistical properties of response time for larger membrane area. But through the phase plane analysis we see that the most inner APT results in the maximal response time, which is the up limit of the average response time. As the membrane area increases to infinitely large, the average
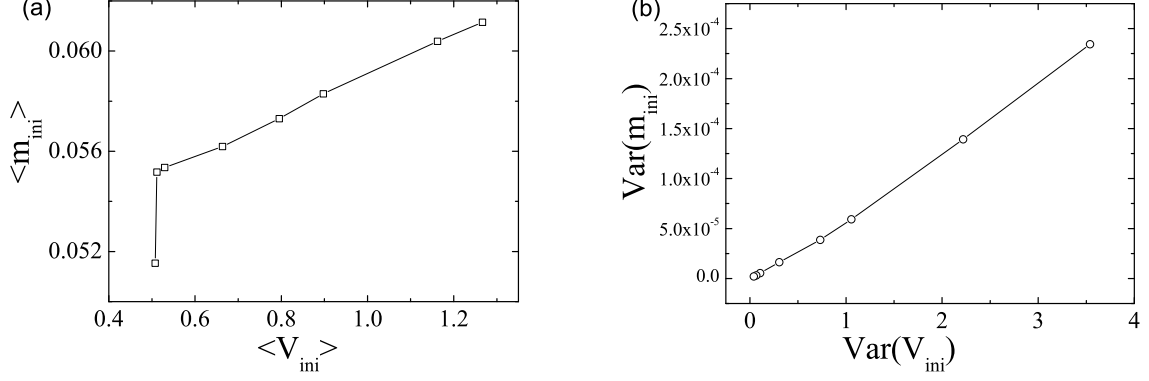
FIG. 4: The distribution of initial states for different membrane areas. (a) The averages of V_{ini} and m_{ini} for different membrane areas. (b) The variances of V_{ini} and m_{ini} for different membrane areas. The eight different dots, from top to bottom in each plot, correspond to membrane area $S = 20, 50, 80, 100, 200, 500, 800, 1000 \, \mu m^2$, respectively.
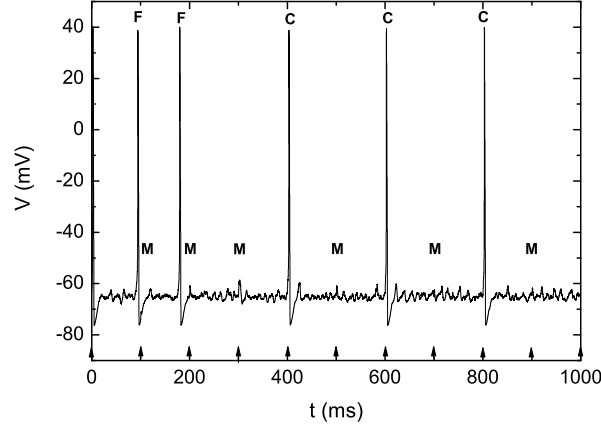

FIG. 5: Trace of the membrane potential of the SHH neuron for transient input pulses with width of $0.1ms$ and height of $5 \, \mu A/cm^2$. The time of occurrence for pulses is marked by arrowheads on the horizontal axis. C: the incidences that the pulse is correctly detected by the neuron; M: the incidences that the neuron does not respond to the pulse; F: the incidences that a spike occurs in the absence of a pulse.

response time will increase gradually to this maximal value. We argue this maximal response time corresponds to the response time of the noise-free HH neuron to the pulse of which the strength to elicit a spike is minimal. In the deterministic HH model, for the pulse input with the minimal strength of $I_0 = 6.92 \, \mu A/cm^2$ and $\delta t = 0.1ms$, the maximal response time we obtained is $5.87ms$, which matches the PSTH peaks' right edges (see curves for $200\mu m^2$ and $1000\mu m^2$ in Fig. 2(a)). This time scale is important for the choosing of the coincidence time window ρ introduced in section IV. If ρ is much larger than the maximal response time the SHH neuron could provide, spontaneous firings will be detected together with the stimulated firings, thus reduce the accuracy of detection. On the contrary, if ρ is far less than it, some stimulated firings will be ignored, so the efficiency of detection is reduced.

IV. THE PERFORMANCE OF PULSE DETECTION

Now, we consider the pulse detection task as a simple computation that a neural system can perform, in which we evaluate the performance of a single SHH neuron as well as a SHH neuron assembly.

The input I_{stim} is modeled as a serial narrow rectangular current pulse with width $\delta t = 0.1ms$ and strength $I_0 = 5 \, \mu A/cm^2$

(see Fig. 5). The input pulse train (the arrowheads on the horizontal axis) is regular with a large time interval $\Delta T = 100ms$. Compared to the membrane time constant, the preceding pulse has no significant influence on the following one. In such an arrangement, as has been discussed above, the SHH neuron has three different responses (marked with different capital letters respectively in Fig. 5) to the pulse train which consists of n equidistant pulses:

(1) C : The neuron generates an action potential immediately (within the time rang of $5ms$) after a pulse is presented, which signifies successful detection of the pulse. We define P_C as the fraction of correctly detected pulses, which is the total number of correctly detected pulses, divided by the total number of input pulses.

(2) M : The neuron fails to fire a spike immediately (within the time rang of $5ms$) after the pulse is presented. If we define P_M as the fraction of missed pulses, then we have $P_M = 1 - P_C$.

(3) F : The neuron fires a spike in the absence of an input pulse (a false positive event). A deterministic HH neuron cannot fire spikes when the stimulus is not applied or if it is below the threshold. However, in the case of channel noise, stochastic effects give rise to spontaneous spiking. To describe the effect of those spontaneous firing spikes on subthreshold pulse detection, we denote P_F as the total number of false positive events divided by the total number of input pulses. Note that P_F can easily exceed 1.

In order to quantify the neuron's response to the pulse train, we define the total error Q for the pulse detection,

$$Q = P_M + P_F. \tag{8}$$

For a longer interval ΔT with fixed n, the false positive events are more likely to occur and the total error grows with increasing ΔT.

Fig. 6(a) shows P_C, P_M, and P_F as a function of the membrane area under the above-mentioned scenario. According to the above PSTH analysis , when the membrane area is rather large, though the system could be displaced by subthreshold pulses to near the threshold, the channel noise is small and can hardly trigger firings, thus P_C is very small and $P_M \approx 1$. The firings triggered by noise alone is even less, so the P_F is smaller than P_C. When the membrane area is small, the channel noise is remarkable, giving large P_C. Meanwhile, due to the high rate of spontaneous firings, P_F is even larger than P_C. So, with increasing membrane area, both P_C and P_F decreases, but P_F drops more quickly than P_C. When the membrane area is larger than about $180\mu m^2$, P_C becomes larger than P_F.

The total error Q as a function of the membrane area is also plotted in Fig. 6(b). As the membrane area increases, due to the rapid decline of P_F, the total error Q drops rapidly. Then, with further increase in membrane area, Q increases and approaches 1 for the major contribution from the fraction of missed pulses. Because Q is basically the summation of ascending P_M curve and descending P_F curve, one can expect a minimal value for it. The minimal value of Q is 0.8746 at $S = 300\mu m^2$. With this optimal membrane area, we see that the neuron achieves balance between detecting pulse input and suppressing spontaneous firings.

It should be noted that the positions for P_C, P_M and P_F curves are dependent on the strength of pulse input I_0, or the interpulse interval ΔT. Changing the pulse strength would change the position of P_C curve, thus the position of P_M in Fig. 6(a). In particular, smaller pulse strength leads to lower position of P_C, thus higher position of P_M(see Fig. 7 of Ref.[18] or Fig. 6 of Ref.[14]). As discussed above, the pulse induced high firing rate would reduce the spontaneous firing rate through refractoriness within the following $10ms$. If ΔT is large compared to refractory period of SHH neuron, this reduction in spontaneous firings is negligible, so the pulse strength would not affect the position of P_F curve. On the contrary, by their definition, P_F, rather than P_C and P_M, is greatly dependent on ΔT. Whatsoever, neither pulse strength nor interpulse interval will not change the overall shape of both P_C and P_F curves. Since the minimal Q is basically the result of summation of ascending P_M curve and descending P_F curve, we argue that there is always a minimal value for Q, and the optimal membrane area for Q differs for different input pulse strength or interpulse interval.

We see that the single neuron has limited capacity for subthreshold signal detection. The channel noise is basically a zero-mean noise, which means the probability for a subthreshold pulse gets enhanced by a positive fluctuation is equal to the probability that it is further suppressed by its negative counterpart. In more detail, the response of the SHH neuron to input current pulses is state-dependent(Fig. 3(c)). Channel noise perturbations enable the system, with equal chance, to be in a high state that the neuron is more likely to fire a spike after pulse is applied, or in a low state that no fires occur. As a result, P_C could never exceed 0.5, and the total error for a single neuron is always larger than 0.5. Indeed, we found in Fig.4 of Ref. [14] that the spike efficiency for subthreshold voltage impulses never exceed 50% and the same conclusion was made in Ref. [18] for external noise. So we see that theoretically, it is unlikely to utilize channel noise to reliably detect subthreshold signals with single neuron. However, in reality, the neuron assembly works in real neural systems rather than in a single neuron. In general, neurons work cooperatively through synaptic coupling. What's more, among various spatiotemporal spike patterns in the neural system, synchronous firing has been most extensively studied both experimentally and theoretically [31, 32]. Believing that neuronal synchronous firing is critical for transmitting sensory information, many investigators have suggested that a major function of cortical neurons is to detect coincident events among their presynaptic inputs (see [33] for more references). Based on this fact, we proposed a neuronal network that can greatly enhance the detection ability of the pulse.
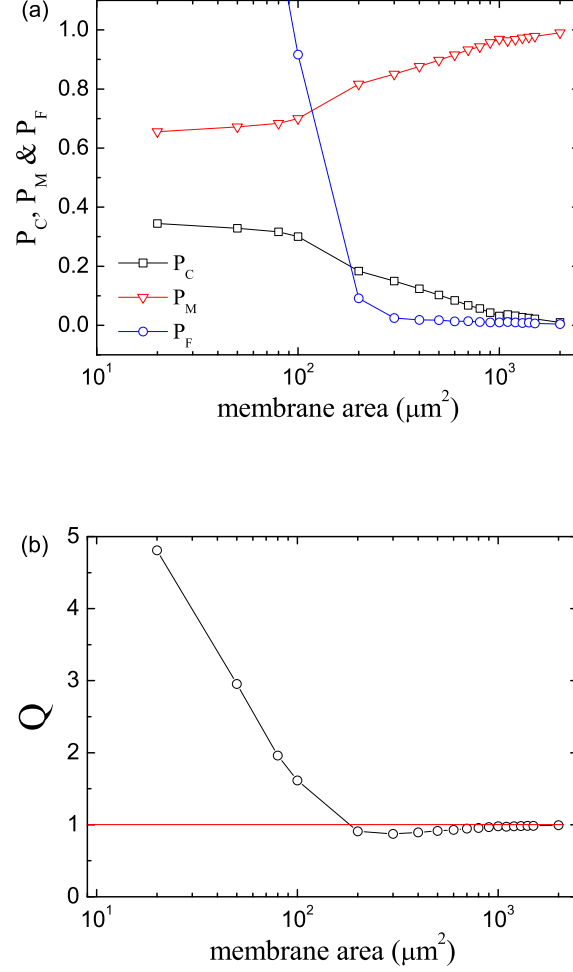
FIG. 6: (Corlor online) The performance of a single neuron in a subthreshold pulse detection task. (a) P_C, P_M, P_F, and (b) total error Q as a function of membrane area.

As shown in Fig. 7, the front layer of the network is composed of globally coupled identical neurons with channel noise. The coupling term has the form of an additional current I_{couple} added to the equation for the membrane potential (see Eq. 1). For the ith neuron, it takes the form

$$I_{couple} = \frac{\varepsilon}{N} \sum_{j=1}^{N}(V_j - V_i), \tag{9}$$

where ε is the coupling strength and V_i is the membrane potential of the ith neuron for $i = 1, \ldots, N$. In our simulations, neurons are weakly coupled, $\varepsilon = 0.005$. And the membrane area of each SHH neuron is set as $S = 200\mu m^2$. Here we chose this value for the membrane area rather than the optimal one so that P_C of a single neuron is relatively large. Thus fewer neurons are needed in our network and the computational cost is consequently reduced. Each SHH neuron in the network receives the same subthreshold pulse train as in the single neuron case. The output spike trains of those neurons S_i ($i = 1, 2, \ldots, N$) are taken as the input of a so-called coincidence detector (CD) neuron. In neural reality, coincidence detection requires complex cellular mechanisms [34, 35]. For simplicity, here we use a phenomenological CD neuron model. The CD neuron is excited when it detects spikes from more than θ neurons within a coincidence time window ρ ($= 5\ ms$, see discussion Sec. V). In other words, θ denotes the detection threshold of the CD neuron. After firing, the CD neuron enters a refractory period of 5 ms. Obviously, given the input spike trains S_i, the output spike train R_θ of the CD neuron is determined by its threshold θ. We also define P_C^{θ} and P_F^{θ} as the fraction of correct detection and false reporting in the network with the CD threshold θ, respectively. Similarly,
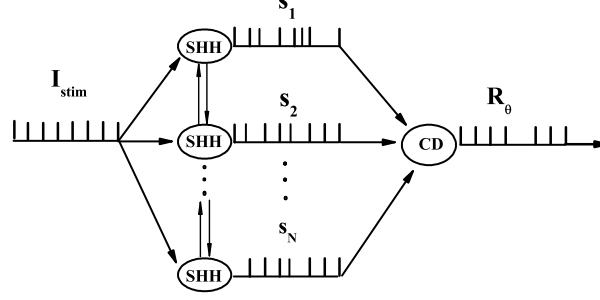
FIG. 7: A schematic diagram of pulse detection with multiple neurons. I_{stim} is the input pulse train. $\mathbf{S}_i$ is the output spike train of the ith SHH neuron for $i = 1, 2, \ldots, N$. CD is the coincidence detector neuron and $\mathbf{R}_\theta$ is its output spike train with synchronous firing detecting threshold θ. Here we demonstrate the case of $\theta = 2$.

Q^θ is defined as the total error of the network with the CD threshold θ.

TABLE II: The performance of the network with optimal sizes for different CD threshold θ.

θ	1	2	3	4	5	6
N_{opt}	5	22	42	62 ~ 65	69 ~ 91	78 ~ 158
Q_{min}	0.725	0.132	0.025	0	0	0
P_C^θ	0.619	0.937	0.998	1.0	1.0	1.0

Fig. 8(a) shows P_C^θ as a function of the number of SHH neurons N for $\theta = 1, 2, 3$. As the number of neurons N increases, all P_C^θ increase quickly to $P_C^\theta = 1$. For larger θ, the increase of P_C^θ becomes slower and requires more neurons to achieve the successful state $P_C^\theta = 1$. However, the enhancement of P_C^θ is at the cost of unexpected improvement in P_F^θ. As shown in Fig. 8(b), with increasing N, P_F^θ is also improved. Note that P_F^θ is able to exceed 1. Comparing Fig. 8(a) with (b), it is obvious that, though both P_C^θ and P_F^θ increase with an increased number of neurons, comparing to P_C^θ, the increasing of P_F^θ is always delayed. Thus, in the case of a small N, the correct detection will not be greatly enhanced though P_F^θ is low. Whereas for large N, one can obtain better performance for correct detection but a cost of a higher P_F^θ. Therefore, we expect to find an optimal N to achieve the best performances for signal detection.

Fig. 8 (c) displays the total error Q^θ as a function of the number of neurons N for different θ. Clearly, the minimal total error Q_{min} or the resonance behavior appears at the network level. For different θ, there exist different optimal numbers of SHH neurons N_{opt} where the performance of pulse detection is at its best. As shown in Table II, with increasing θ, Q_{min} decreases while the corresponding N_{opt} increases. Simultaneously, P_C^θ corresponding to the N_{opt} increases. If θ is large enough, the Q_{min} becomes nearly zero (< 0.001) in a wide range of SHH neuron numbers. Theoretically, by further enhancing the detection threshold and involving more neurons, the zero value of Q_{min} could appear in a wider range of SHH neuron numbers.

We define syn-firing probability P^θ as the probability that θ or more than θ SHH neurons fire in a time interval. Supposing the firing probability of each independent SHH neuron (ignoring the couplings between them) in a time interval is p, then syn-firing probability P^θ in this time interval is described by cumulative distribution function for a binomial distribution, i.e.,

$$P^\theta = \sum_{\alpha=\theta}^{N} \frac{N!}{\alpha!(N-\alpha)!} p^\alpha (1-p)^{N-\alpha}, \tag{10}$$

where $p^\alpha(1-p)^{N-\alpha}$ is the probability that only α neurons fire at the same time, and $C_\alpha^N = \frac{N!}{\alpha!(N-\alpha)!}$ is the number of ways of picking α neurons from population N. So $\sum_{\alpha=\theta}^{N} \frac{N!}{\alpha!(N-\alpha)!}$ is the total number of ways of selecting θ or more than θ neuron out of population N. Then the firing probability for CD neuron with threshold θ and refractoriness is written as

$$P_{CD}^\theta = P^\theta - (influence\ of\ past\ perturbations), \tag{11}$$

where the last term represents the suppression of past firings on present firing probability through refractoriness, which is proportional to the probability for past firing events [36]. This term can be cancelled because it often acts as small perturbations, and
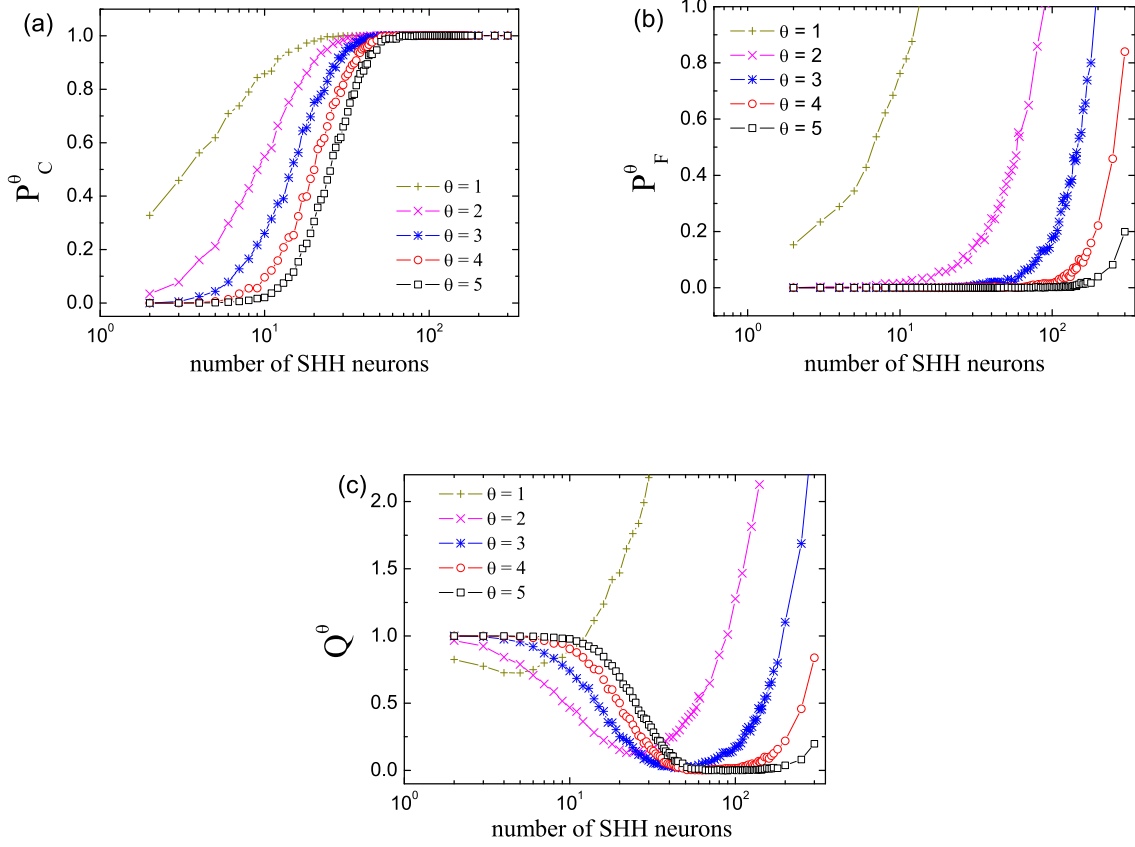
FIG. 8: (Color online) Detection of subthreshold signals with the neuronal network for the CD threshold $\theta = 1, 2, ..., 5$. (a) P_C^θ, (b) P_F^θ, and (c) Q^θ as a function of number of SHH neurons.

does not bring qualitative changes to firing probabilities of CD neuron statistically. So in the following analysis, for simplicity, we take $P_{CD}^\theta \approx P^\theta$.

From Fig. 9(a) we see that P^θ, thus P_{CD}^θ increases with increasing p, the firing probability of each neuron. So when pulses are applied to the SHH neuron, the firing probability of CD neuron is larger than that caused by channel noise alone, because the firing probability of each SHH neuron is enhanced. By increasing the number of SHH neurons, no matter p is large or small, P^θ, thus P_{CD}^θ increases(Fig. 9(b)). Since as in the single neuron case, P_C^θ is proportional to P_{CD}^θ in response to subthreshold pulses, and P_F^θ is proportional to P_{CD}^θ induced by channel noise alone. P_C^θ and P_F^θ rise, but P_M^θ declines (not shown) as the number of SHH neurons increases. Therefore, as a result of summation of declining P_M^θ curve and ascending P_F^θ curve, a minimum of the total error Q^θ is warranted.

As shown in Fig. 9(c), with the increasing of θ, P^θ drops, and for small p, P^θ drops more quickly. So both P_C^θ and P_F^θ curves move right-down in Fig. 8 (a) and (b), and P_M^θ curves move right-up(not shown). Thus, Q_{min} curves would move rightward in Fig. 8(c). Since for single SHH neuron, its firing probability is low when pulse inputs are absent, P_F^θ curves move more rapid than the P_M^θ curves. As a result, the Q^θ curves become wider, and move also downward in Fig. 8(c) as θ increases. So we see that the drop of Q_{min} is warranted and $Q_{min} = 0$ is expected to achieve in a wide range of SHH neuron number when θ is large enough.

V. DISCUSSION AND CONCLUSION

In this paper, we used the stochastic version of Hodgkin-Huxley neuron model in which channel noise is the only source of noise, and discussed the possibility of detecting subthreshold signals with channel noise.

First, we studied the response property of the single SHH neuron to the subthreshold transient input pulses. The main result
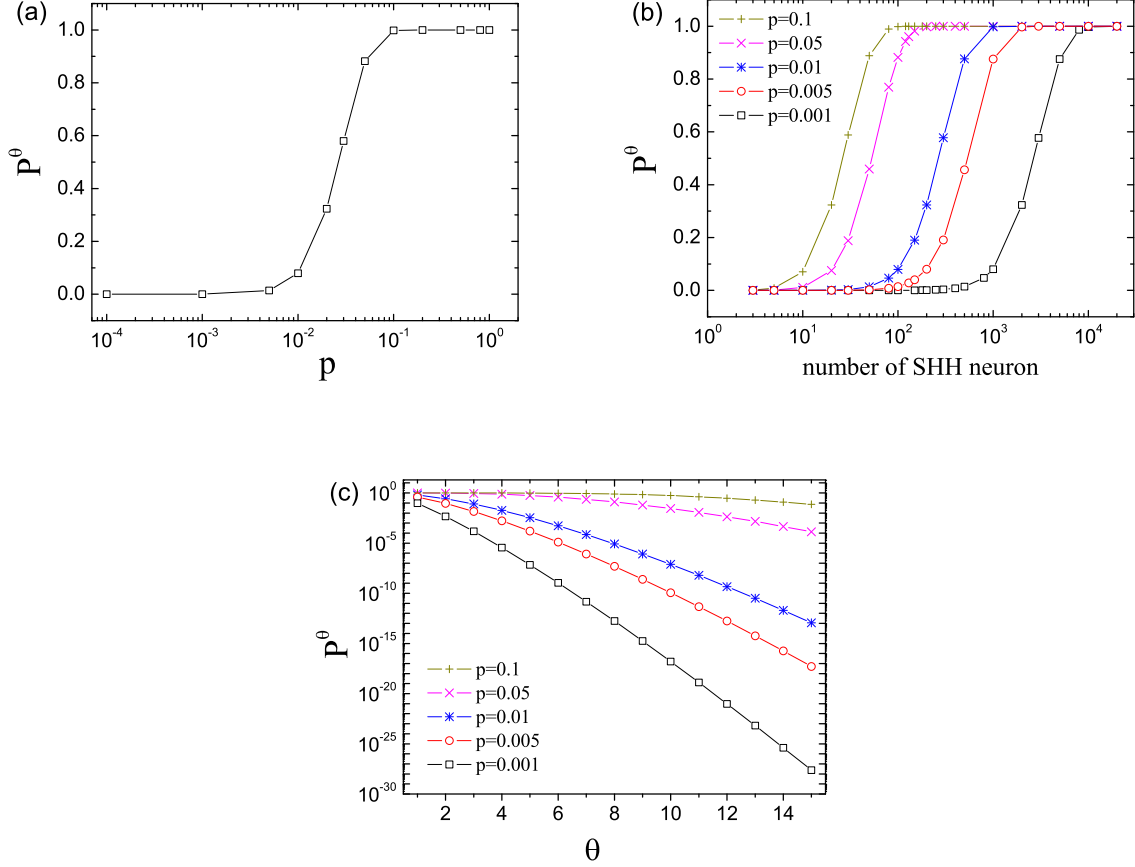
FIG. 9: (Corlor online) The syn-firing probability P^θ of the network calculated from Eq. 10. (a) P^θ as a function of p, the firing probability of each SHH neurons. $\theta = 3$, $N = 100$. (b) P^θ as a function of number of SHH neurons for different p. $\theta = 3$. (c) P^θ as a function of θ for different firing probability of each SHH neurons p.

is that the SHH neuron fires spikes with a higher rate over its average level in response to a subthreshold stimulus. The average response time decreases but its variance increases as the channel noise amplitude increases (or with decreasing membrane area). We further found the existence of an up limit for the average response time. From phase plane analysis we see that this up limit should be predictable for threshold systems with any zero-mean noise, as the noisiness decreases. This results means the response time is very sensitive to the membrane area, because a small decreasing of membrane area would lead to remarkable decreasing in mean response time and increasing in its variance.

Adair has demonstrated the stochastic resonance in ion channels as the output response (in the probability of action potential spikes, which is equivalent to P_C in our paper.) from small input potential pulses across the cell membrane is increased by added noise, but falls off when the input noise becomes large. However, to evaluate the reliability of subthreshold signal detection, one must consider not only the response to subthreshold signals but also the spontaneous firings, because from the standpoint of a neuron, those two kinds of output make no difference. In this paper, we endowed the SHH with a simple pulse detection scenario and calculated the total error Q. We found that a minimal Q and the corresponding optimal membrane area (noise). So we argue that to maximize the detection ability, the strategy a neuron should take is balancing between response to pulses and rejecting spontaneous firings, rather than improving the response to pulses alone with optimal noise as Adair demonstrated. As we argued, the first strategy allow to achieve the minimal Q for different pulse strengths, unlike the second one with which is in effect only for large pulse strength (see Fig. 6 in Ref. [14]). However, even with the first strategy, we found the detection ability of a single neuron is non-credible because Q cannot be larger than 0.5. Though the results are obtained with channel noise, we argue the conclusion should be general for any zero-mean noise.

The current SHH model is only an approximation to a much more complex reality. For example, it has presumed that the channel dynamics are Markov chain process, they act independently, and the gating currents related to the movement of gating charges are negligible. However, those presumptions are not always tenable. For example, Schmid has shown that the gating

currents drastically reduce the spontaneous spiking rate if the membrane area is sufficiently large [37]. So our results should be reinvestigated with consideration of those factors. But we think those factors would not bring qualitative changes to our results, thus the general conclusions still hold.

We then investigated the subthreshold signal detection in a neuronal network that concerns a coincidence detection neuron. We found by enhancing coincidence detection threshold and increasing the SHH neurons, the detection ability is greatly improved. It suggests that channel noise may play a role in information processing in the neural network level. In addition, corresponding to different coincidence detection thresholds, there exist an optimal number of neurons at which the total error is at its minimum. We have seen that this is also the result of balancing between responding to pulses and rejecting spontaneous firings. Since this so-called double-system-size resonance phenomenon has been rarely reported [38], our work provides an example of such an observation. In particular, with sufficiently large coincidence detection threshold, the total error is zero in a wide range of SHH neuron number, which means the detection ability of this network could be robust against variance of neuron number caused by cell production and death.

We have shown that the reliable detection of subthreshold signals with the network is predictable with probability theory, as long as each front layer neuron exhibits higher firing probability in response to signals than that induced by noise. Weak signal detection is also important in practice. For example, mobile communications dictates the use of low power detection to prolong the battery life. So our work suggests a possible way to design reliable stochastic resonance detector for weak signals [39].

[1] D. Paré, E. Shink, H. Gaudreau, A. Destexhe, and E. J. Lang, J. Neurophysiol. **79**, 1450 (1998).
[2] M. Volgushev and U. T. Eysel, Science **290**, 1908 (2000).
[3] L. Gammaitoni, P. Hänggi, and P. Jung, Rev. Mod. Phys. **70**, 223 (1998).
[4] W. C. Stacey and D. M. Durand, *Stochastic resonance in simulated and in vitro hippocampal CA1cells. Engineering in Medicine and Biology* In: *21st Annual Conf. and the 1999 Annual Fall Meeting of the Biomedical Engineering Soc.* **1**, 364 (1999).
[5] W. C. Stacey and D. M. Durand, J. Neurophysiol. **83**, 1394 (2000).
[6] W. C. Stacey and D. M. Durand, J. Neurophysiol. **86**, 1104 (2001).
[7] J. A. White, R. Klink, and A. Alonso, J. Neurophysiol. **80**, 262 (1998).
[8] E. Schneidman, B. Freedman, and I. Segev, Neural Comput. **10**, 1679 (1998).
[9] E. Schneidman, I. Segev, and N. Tishby, *Information capacity and robustness of stochastic neuron models. In S. A. Solla* In: *Advances in Neural Information Processing*, edited by T. K. Leen and K. R. Müller (Cambridge: MIT Press, 2000), pp. 178-184.
[10] S. Schreiber, J. M. Fellous, and P. Tiesinga, J. Neurophysiol. **91**, 194 (2004).
[11] J. A. White, J. T. Rubinstein, and A. R. Kay, Trends Neurosci. **23**, 131 (2000).
[12] P. Jung and J. W. Shuai, Europhys. Lett. **56**, 29 (2001).
[13] G. Svirskis, V. Kotak, D. H. Sanes, and J. Rinzel, J. Neurophysiol. **91**, 2465 (2004).
[14] R. K. Adair, Proc. Natl. Acad. Sci. USA **100**, 12099 (2003).
[15] G. Schmid, I. Goychuk, and P. Hänggi, Europhys. Lett. **56**, 22 (2001).
[16] L. C. Yu, Y. Chen, and P. Zhang, Eur. Phys. J. B **59**, 249 (2007).
[17] J. Rinzel and G. B. Ermentrout, *Analysis of neural excitability and oscillations* In:*Methods in Neuronal Modeling: From Synapses to Networks*, edited by C. Koch and I. Segev, (Cambridge MA: MIT Press. 1989), pp. 135-169.
[18] G. Wenning, T. Hoch, and K. Obermayer, Phys. Rev. E **71**, 021902 (2005).
[19] A. L. Hodgkin and A. F. Huxley, J. Physiol. **117**, 500 (1952).
[20] P. Dayan and L. F. Abbott, *Theoretical neuroscience: computational and mathematical modeling of neural systems* (USA: MIT press, USA, 2001).
[21] R. F. Fox, Biophys. J. **72**, 2068 (1997).
[22] S. Y. Zeng and P. Jung, Phys. Rev. E **70**, 011903 (2004).
[23] H. C. Tuckwell and F. Y. M. Wan, Physica A **351**, 427 (2005).
[24] S. Boris, G. Gutkin, B. Ermentrout, and D. A. Reyes, J. Neurophysiol. **94**, 1623 (2005).
[25] H. Hasegawa, Phys. Rev. E **66**, 021902 (2002).
[26] S. L. Ginzburg and M. A. Pustovoit, Physica A **369**, 354 (2006).
[27] G. Svirskis, V. Kotak, D. H. Sanes, and J. Rinzel, J. Neurosci. **22**, 11019 (2002).
[28] D. Brown, J. Feng, and S. Feerick, Phys. Rev. Lett. **82**, 4731 (1999).
[29] R. VanRullen and S. J. Thorpe, Trends Neurosci. **28**, 1 (2005).
[30] H. C. Tuckwell, Biosystems **80**, 25(2005).

[31] H. Kitajima and J. Kurths, Chaos **15**, 023704 (2005).

[32] L. M. Ward, Trends Cong. Sci. **7**, 553 (2003).

[33] S. A. Roy and K. D. Alloway, J. Neurosci. **21**, 2462 (2001).

[34] D. H. Edwards, S. R. Yeh, and F. B. Krasne, Proc. Natl. Acad. Sci. USA **95**, 7145 (1998).

[35] G. J. Stuart and M. Häusser, Nat.: Neurosci. **4**, 63 (2001).

[36] A. Herrmann and W. Gerstner, J. Comp. Neurosci. **11**, 135 (2001)

[37] G. Schmid, I. Goychuk and P. Hänggi, Phys. Biol. **3**, 248 (2006).

[38] M. S. Wang, Z. H. Hou, and H. W. Xin, ChemPhysChem **5**, 1602 (2004).

[39] A. A. Saha and G. V. Anand, Signal Processing **83**, 1193 (2003).